Soft Matter

RSC Publishing

PAPER

View Article Online
View Journal | View Issue

Cite this: *Soft Matter*, 2013, **9**, 6482

Molecular dynamics simulations of PPI dendrimer–drug complexes†

Vaibhav Jain,[a] Vishal Maingi,[b] Prabal K. Maiti*[b] and Prasad V. Bharatam*[c]

Dendrimeric nanoparticles are potential drug delivery devices which can enhance the solubility of hydrophobic drugs, thus increasing their bioavailability and sustained release action. A quantitative understanding of the dendrimer–drug interactions can give valuable insight into the solubility and release profile of hydrophobic drug molecules in various solvent conditions. Fully atomistic molecular dynamics (MD) simulations have been performed to study the interactions of G5 PPI^{EDA} (G5 ethylenediamine cored poly(propylene imine)) dendrimer and two well known drugs (Famotidine and Indomethacin) at different pH conditions. The study suggested that at low pH the dendrimer–drug complexes are thermodynamically unstable as compared to neutral and high pH conditions. Calculated Potential of Mean Force (PMF) by umbrella sampling showed that the release of drugs from the dendrimer at low pH is spontaneous, median release at neutral pH and slow release at high pH. In addition, Molecular Mechanics Poisson–Boltzmann Surface Area (MM-PBSA) binding free energy calculations were also performed at each umbrella sampling window to identify the various energy contributions. To understand the effect of dendrimer chemistry and topology on the solubility and release profile of drugs, this study is extended to explore the solubility and release profile of phenylbutazone drug complexed with G3 poly(amidoamine) and G4 diaminobutane cored PPI dendrimers. The results indicate that the pH-induced conformational changes in dendrimer, ionization states, dendrimer type and pK_a of the guest molecules influence the free energy barrier and stability of complexation, and thus regulate drug loading, solubility and release.

Received 9th February 2013
Accepted 16th May 2013

DOI: 10.1039/c3sm50434d

www.rsc.org/softmatter

1 Introduction

Studies on nanotechnology based drug delivery systems are gaining momentum as they have potential to augment the therapeutic effect or to reduce the toxicity of drugs without any need for tailoring the pharmacophoric features.[1] Among the various nano-scopic architectures, dendrimers are emerging as versatile carrier systems in the field of biomedical and pharmaceutical sciences,[2–4] because of their unique structural properties and biocompatibility with other macromolecular targets.[5,6] These distinctive features of dendrimers offer numerous advantages over the traditional linear polymers, and thus make dendrimers as attractive polymeric systems suitable for a wide spectrum of applications (drug delivery,[7,8] siRNA/DNA delivery,[9–14] cancer diagnostics,[15] and in catalysis[16]). Among the different classes of dendrimers, poly(amidoamine) (PAMAM),[17] poly(propylene imine) (PPI)[18] and poly(propyl ether imine) (PETIM)[19,20] are the most widely explored dendrimers for pharmaceutical applications because of their commercial availability, high drug loading capacity and ease of synthesis in addition to the above mentioned attributes.

Numerous experimental studies have been carried out on dendrimers to explore their potential as nanovectors in drug delivery, in order to enhance the solubility and bioavailability of drugs,[21,22] decreased toxicity,[8] sustained/controlled release[23,24] and to achieve targeted drug delivery.[25,26] Pharmaceutical compounds can be either physically associated with the dendrimer (surface/cavities) to render the noncovalent complex or covalently attached with the peripheral groups of dendrimer to yield conjugates.[27] In the last decade, dendrimers emerged as promising tools for the encapsulation and the delivery of poorly water soluble class II drugs (Biopharmaceutical Classification

[a]*Department of Pharmacoinformatics, National Institute of Pharmaceutical Education and Research, Sector 67, S.A.S. Nagar, Punjab 160 062, India*

[b]*Centre for Condensed Matter Theory, Department of Physics, Indian Institute of Science (IISc), Bangalore 560 012, Karnataka, India. E-mail: maiti@physics.iisc.ernet.in; Fax: +91-80-2360-2602; Tel: +91-80-2293-2865*

[c]*Department of Medicinal Chemistry, National Institute of Pharmaceutical Education and Research (NIPER), Sector 67, S.A.S. Nagar, Punjab 160 062, India. E-mail: pvbharatam@niper.ac.in; Fax: +91-172-2214692; +91-9417503172; Tel: +91-172-2292018*

† Electronic supplementary information (ESI) available: Building G5 PPI^{EDA} dendrimer using DBT, computational details for ligand processing, molecular docking and MM-PBSA methodology, quantum chemical analysis of protonated Famotidine, hydrogen bond analysis between peripheral amines and water, snapshots of G5 PPI^{EDA}–Famo and G5 PPI^{EDA}–Indo complexes at different time intervals for various pH conditions, MM-PBSA energy components plot for G5 PPI^{EDA}–Indo complexes at different pH conditions, hydrogen bond analysis between drug Indo and G5 PPI^{EDA} dendrimer and radius of gyration for drug loaded dendrimers. See DOI: 10.1039/c3sm50434d

System[28]) which are characterized by poor solubility and high permeability.[27,29] The dendrimers with hydrophobic interior and hydrophilic periphery possess container properties and also show micelle-like behavior[30] which is responsible for their solubilizing effect.[31,32] Dendrimer-mediated solubility enhancements of hydrophobic drugs mainly depend on factors such as generation size, dendrimer concentration,[33,34] pH,[35,36] architecture of the core, temperature, surface charge and terminal functionality.[21] Moreover, the pK_a, size, functional groups and nature of hydrophobes also play an important role in the process of solubilization.[35,37,38] The possible mechanisms responsible for the dendrimer mediated solubility enhancement include a variety of non-bonding interactions such as hydrophobic, hydrogen bonding and electrostatic or ion pairing.[39,40] Several groups around the globe have performed extensive experimental investigation on the factors affecting the solubilization *via* dendrimer and proposed the probable mechanisms.[21–24,32–44]

The structural differences in the interior pockets of the dendrimer also exhibit interesting physicochemical implications for the host behaviour and its interaction with the guest molecule.[42,43,45] Previous studies demonstrated that the internal microenvironment of PPI is nonpolar while PAMAM has relatively polar pockets.[46] To explore further in this area, recently Shao *et al.*[44] carried out comparative study on various aspects (drug loading efficiency, host–guest chemistry, complex stability, release profile and cytotoxicity) of G3 PAMAM and G4 diaminobutane cored PPI dendrimer (PPI^{DAB}). It was observed that non-steroidal anti-inflammatory drug (NSAID) phenylbutazone (Pbz, pK_a = 4.5) release is much slower from the G3 PAMAM dendritic matrix than from the G4 PPI^{DAB} dendrimer.[44] To investigate the nature of hydrophobes and the effect of pH on dendrimer mediated solubilization, Jain and co-workers[35] considered weakly basic (Famotidine (Famo), pK_a 7.1), weakly acidic (Indomethacin (Indo), pK_a 5.0), and amphoteric (Amphotericin B, pK_a 5.7 and 10.0) drug molecules encapsulated in the G5 ethylenediamine cored PPI dendrimer (PPI^{EDA}). Phase solubility studies revealed that solubility of all the drugs was significantly enhanced at neutral (~7.4) and high pH (~10.0) but not at low pH (~4.0).[35]

Computational studies play a complementary role in the design and optimization of dendrimer-based host–guest systems.[4] In one of the earlier studies, Goddard and co-workers[47] performed MD simulations to examine the encapsulation of guest Bengal Rose molecules in the Meijer dendrimer box (DBox) formed by the capping of 64 peripheral amines of a G5 PPI dendrimer. Posocco and co-workers[48] studied the binding free energies of two guest molecules with two series of naphthyridine-based dendrimers using Molecular Mechanics Poisson–Boltzmann Surface Area (MM-PBSA), and the calculated values were found to be in good agreement with the experimental results. Recently, to evaluate the quantitative structure–affinity relationship in a dendrimer–drug system, their interaction energies were calculated using the Metropolis Monte Carlo algorithm and semiempirical quantum mechanical methods.[49] Lewis and Ganesan[50,51] implemented a self-consistent field theory model to gain insight into the mechanism behind the solubilization of weakly acidic drugs *via* dendrimeric architectures. The individual and synergistic effects of excluded volume interactions, electrostatic attractions, and enthalpic interactions (hydrophobic and hydrogen bonding) on the encapsulation efficiency of dendrimers were explored. In our previous study,[52] the release profile of soluble and insoluble ligands from the G5 PAMAM dendrimer at neutral pH condition was examined using Potential of Mean Force (PMF) calculations. The results showed that energy barriers for the insoluble ligands are more as compared to the soluble ligands. Some other studies are also available in the literature which provides molecular level description of dendrimer–guest interactions.[53–64]

In the present MD simulations study, an attempt has been made to compare and understand the solubility and release profile of hydrophobic drugs from G5 PPI^{EDA} dendrimer at different pH conditions and with different dendrimer architectures (G3 PAMAM *vs.* G4 PPI^{DAB}). The equilibrated structures of G5 PPI^{EDA} (corresponding to low, neutral and high pH) were obtained from the full atomistic MD simulations and validated by calculating several structural properties. Famo and Indo drug molecules were then encapsulated in G5 PPI^{EDA} separately and their complexes were subjected to MD simulations at all the three pH conditions. Furthermore, the release profile of these drugs from the dendrimer has been examined at different pH conditions by PMF calculations using umbrella samplings.[65] In addition, binding free energy calculations were also performed to evaluate the contribution of different intermolecular forces (electrostatic and van der Waals) in the overall binding. Finally, we have also performed MD simulations to understand the differences in the aqueous solubility and release profile of Pbz drug complexed with G3 PAMAM and G4 PPI^{DAB} dendrimers.[44]

2 Materials and methods

2.1 Dendrimer building and ligands processing

The initial configuration of G5 PPI^{EDA} (corresponding to high, neutral and low pH) and G4 PPI^{DAB} dendrimers (corresponding to neutral pH) with Restrained Electrostatic Potential (RESP) charges was generated using Dendrimer Builder Toolkit[66] (DBT) and AMBER.[67] The results of the acid–base titration experiments[68–70] performed on PPI dendrimers revealed that they exhibit different levels of protonation at three different pH conditions. The pK_a value for the primary and tertiary amines of the PPI dendrimer is reported to be around 9.75 and 6.10 respectively.[71] At high pH the dendrimer is fully non-protonated; at neutral pH all the primary amines present at the periphery and the tertiary amines present in the alternative layers are protonated *i.e.* 2/3 protonation; at low pH both the primary as well as tertiary amines are fully protonated (Table 1). Accordingly, to mimic the experimental conditions, different levels of protonation were considered while building the dendrimers using DBT. The equilibrated geometry of G3 PAMAM dendrimer (corresponding to neutral pH) was obtained from our previous work.[66] The pK_a value for the primary and tertiary amines of the PAMAM dendrimer is around 9.50 and 6.50 respectively.[72] For PAMAM dendrimer at neutral pH, all the

Table 1 Details of the simulation conditions and properties of G5 PPI^{EDA} dendrimer at high, neutral and low pH[a]

pH	Protonation of amines	No. of G5 PPI atoms	Molecular formula	Molecular weight	No. of waters	Box size (Å)	Charge of PPI	No. of Cl^-
High	Primary – NP Tertiary – NP	1376	$C_{374}H_{876}N_{126}$	7140	4710	58.53	0	0
Neutral	Primary – P Tertiary – 2/3P	1460	$C_{374}H_{960}N_{126}$	7225	5199	60.51	84	84
Low	Primary – P Tertiary – P	1502	$C_{374}H_{1002}N_{126}$	7267	5497	61.58	126	126

[a] NP: non-protonated, P: protonated.

peripheral primary amines were considered as protonated and tertiary amines as non-protonated.

Details of the dendrimer building are included in the ESI.† The residues used for building G5 PPI^{EDA} are presented in Fig. S1 and S2,† whereas a complete flow chart for building is presented in Fig. S3.† GAFF (General Amber Force Field) atom types and RESP partial atomic charges of both protonated and non-protonated residues are shown in Tables S1–S3.† Likewise for building dendrimer–drug complexes, appropriate charged and uncharged species of drug molecules at low, neutral and high pH conditions were considered (Table 2). The structures of drug molecules along with the preferred protonated or deprotonated sites are depicted in Fig. 1. GAFF atom types and RESP partial atomic charges of drug molecules are mentioned in Tables S4–S6† respectively for the benefit of the readers. In the case of Famo, three protonation sites are possible (Fig. S4†), thus quantum chemical calculations were performed in the gas phase as well as in the presence of implicit solvent (water, CPCM model) to identify the most plausible protonated structure (details given in ESI†).

2.2 Molecular dynamics simulations

Full atomistic MD simulations were performed on G5 PPI^{EDA} (low, neutral and high pH) and G4 PPI^{DAB} (neutral pH) dendrimers using water as an explicit solvent. All the simulations were carried out using AMBER 10 (ref. 67) software package with GAFF force field.[73] Initially, the built dendrimer structures were loaded in *xleap* and were immersed in an octahedral water box using a TIP3P water model[74] by choosing a 10 Å solvation shell. In order to neutralize the positive charges on the dendrimer at neutral and low pH, appropriate numbers of Cl^- counterions were added (Table 1). The solvated neutral structures were then subjected to 1000 steps of steepest descent minimization, followed by 2000 steps of conjugate gradient minimization. During this minimization the dendrimer molecule was kept fixed in its starting conformation using harmonic restraints with a force constant of 500 kcal mol^{-1} $Å^{-2}$. This helped the water molecules to reorganize to remove bad contacts with the dendrimer molecule. Finally 5000 steps of conjugate gradient minimization was carried out while decreasing the force constant of the harmonic restraints from 20 kcal mol^{-1} $Å^{-2}$ to zero in steps of 5 kcal mol^{-1} $Å^{-2}$.

The minimized structure was initially subjected to 40 ps of MD and the system was gradually heated from 0 to 300 K using weak 20 kcal mol^{-1} $Å^{-2}$ harmonic restraints on the solute to its

Table 2 Ionization states of Famo, Indo and Pbz drug molecules at different pH conditions

	Ionization state		
pH	Famo ($pK_a = 7.1$)	Indo ($pK_a = 5.7$)	Pbz ($pK_a = 4.5$)
High (~10)	Neutral	Deprotonated	Deprotonated
Neutral (~7.4)	Neutral	Deprotonated	Deprotonated
Low (~4)	Protonated	Neutral	Neutral

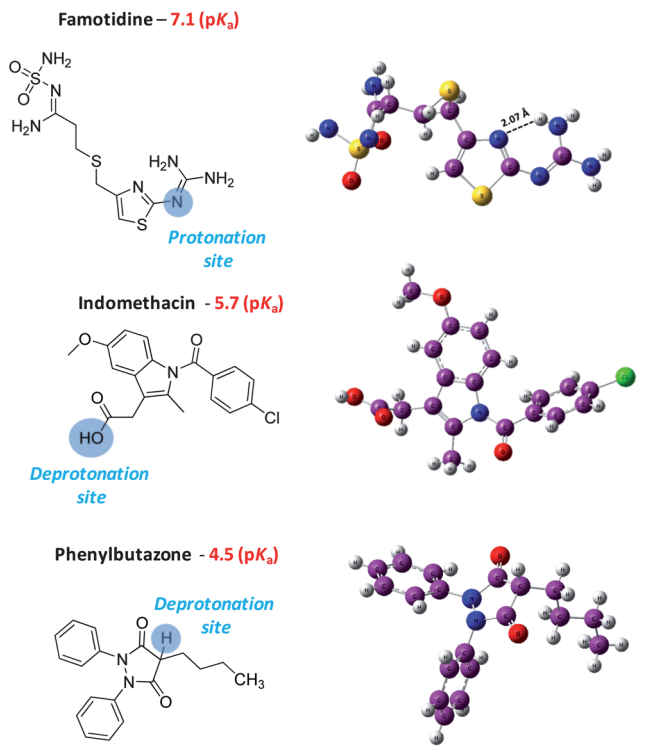

Fig. 1 2D and 3D structure representations of Famo (CSD Refcode: FOGVIG01, showing intramolecular hydrogen bonding), Indo (CSD Refcode: INDMET03) and Pbz (CSD Refcode: JAJKUB) drug molecules along with their respective pK_a values. Blue circles represent the preferred protonation or deprotonation sites in drug molecules. For GAFF atom types and RESP partial atomic charges please refer Tables S4–S6 in the ESI.†

starting structure. This allows slow relaxation of the built dendrimer structure. Subsequently, MD was performed under constant volume–constant temperature (NVT) conditions using less restraint on the solute and then 2 ns of unconstrained NVT MD was carried out to equilibrate the system at 300 K. Finally, 18 ns long constant pressure-constant temperature (NPT) equilibrium dynamics was performed at 300 K and 1 atm pressure; with temperature regulation achieved using the Berendsen weak coupling method (1 ps time constant for heat bath coupling and 0.5 ps for pressure relaxation time).[75] Equations of motion were solved using the Verlet leapfrog algorithm,[76] with an integration step of 2 fs and the trajectory snapshots were saved after each ps. In addition, SHAKE constraints[77] using a geometrical tolerance of 5×10^{-4} Å were imposed on all covalent bonds involving hydrogen atoms. The non-bonded cutoff was kept at 9 Å, and long-range electrostatic interactions were treated by the Particle-Mesh Ewald (PME) method.[78]

Once equilibrated structures of the dendrimers were obtained, they were further utilized to make dendrimer–drug complexes by the molecular docking approach (particulars given in ESI†). The complexes were immersed in an octahedral water box using the TIP3P water model[74] by choosing a 10 Å solvation shell. In order to ensure electrical neutrality of the system, sufficient numbers of Cl^- counterions were added to G5 PPI^{EDA}–Famo and G5 PPI^{EDA}–Indo complexes at neutral and low pH. Moreover, in the case of G5 PPI^{EDA}–Indo (neutral and high pH), G3 PAMAM–Pbz (neutral pH) and G4 PPI^{DAB}–Pbz (neutral pH) complexes, one Na^+ was also added (since Indo and Pbz carry −1 charge). The simulation protocol adopted for these complexes was the same as implemented in the case of the drug unloaded dendrimer. *Ptraj* module of Amber tools and VMD7.6 (ref. 79) were used for the analysis of trajectories.

2.3 Potential of Mean Force (PMF) and MM-PBSA calculations

PMF calculations employing umbrella sampling[65] and the Weighted Histogram Analysis Method (WHAM)[80,81] were performed to generate a free energy profile along the reaction coordinate defined as the dendrimer and drug center-of-mass (COM) separation distance. In the present study we have followed a similar protocol reported in our previous work[52] with PAMAM–drug interactions. The pathway between the two endpoints (COM separation distance) was chosen for pulling the ligand out of the complex into the bulk solvent. For umbrella sampling initial coordinates were obtained from the restart file of 1 ns NVT MD run. Each umbrella window was obtained with an increment of 1 Å from the previous window (starting from the equilibrated COM separation distance) and the sampling time in each window was 1 ns. A harmonic potential with a spring constant of 2 kcal mol^{-1} $Å^{-2}$ was provided for umbrella sampling. The resulting equilibrated structure obtained for each window was used as starting coordinates for the next window. To consider the interactions closer to the core of dendrimer some umbrella samples were also collected by pushing the ligand *i.e.* decreasing the initial COM separation distance. The total length of the simulation run along with the starting equilibrated COM separation distance between dendrimer and drug is presented in Table 3. The reaction coordinate *versus* time was recorded during all production runs and subsequently used with WHAM to calculate the PMF. All the WHAM calculations were performed at 300 K using a convergence tolerance of 0.0001 kcal mol^{-1}.

Table 3 Comparison of various complexes with respect to their starting configurations in terms of distance

Complex	Starting COM separation distance[a] (Å)	Reaction coordinate (Å)	Duration (ns) for umbrella sampling; each window size being 1 ns
G5 PPI^{EDA}–Famo (low pH)	7.23	2 to 24	23
G5 PPI^{EDA}–Famo (neutral pH)	5.57	2 to 24	23
G5 PPI^{EDA}–Famo (high pH)	7.23	2 to 24	23
G5 PPI^{EDA}–Indo (low pH)	10.39	2 to 24	23
G5 PPI^{EDA}–Indo (neutral pH)	5.99	2 to 29	28
G5 PPI^{EDA}–Indo (high pH)	4.52	2 to 24	23
G3 PAMAM–Pbz (neutral pH)	2.80	2 to 20	19
G4 PPI^{DAB}–Pbz (neutral pH)	5.46	2 to 20	19

[a] COM of the ligand considering all atoms and COM of dendrimer considering only central five residues (core 'aaa' and four 'bbb' attached to 'aaa' core).

The binding free energy ΔG_{BIND} of each dendrimer–drug complex in the solvent was estimated *via* the widely used MM-PBSA[82] method implemented in Amber 10 (for details please refer ESI†).[67] The applicability of the MM-PBSA methodology for predicting the binding free energy of dendrimer and guest molecules is well established in the literature.[9,48,83–86] The calculations were performed on each of the umbrella window (each of 1 ns duration for the last 200 snapshots) of PMF corresponding to total 23–28 windows in the case of G5 PPI^{EDA}–Famo and G5 PPI^{EDA}–Indo at all the three pH conditions; 19 windows in the case of G3 PAMAM–Pbz and G4 PPI^{DAB}–Pbz (Table 3) at neutral pH conditions.

3 Results and discussion

3.1 Influence of pH on G5 PPI^{EDA} dendrimer and its complex with Famo and Indo

3.1.1 Structural properties assessment of G5 PPI^{EDA} dendrimer

Size of dendrimers. The size of nanoparticles like dendrimer is a very important aspect that needs to be considered for its effective use in the drug delivery and other biomedical applications.[87] To quantify the size of G5 PPI^{EDA} dendrimer at various

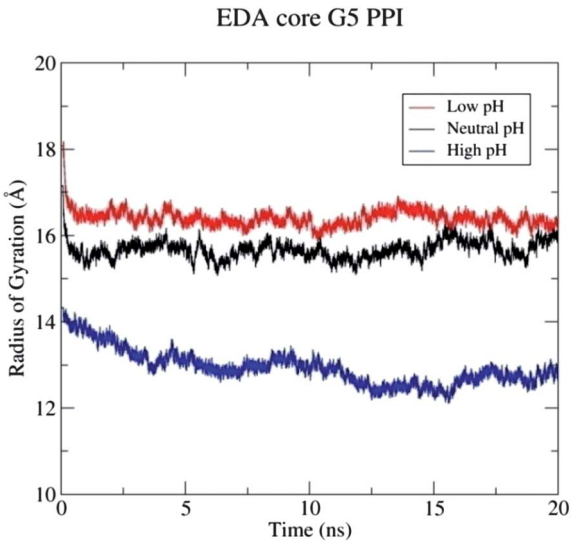

Fig. 2 Time evolution of radius of gyration (R_g) of the G5 PPI^{EDA} dendrimer at high, neutral and low pH conditions for the whole simulation run (each snapshot being saved at 1 ps).

pH conditions, radius of gyration (R_g) has been calculated and plotted with respect to time (Fig. 2). It can be observed from the graphs that simulation time is long enough to attain the equilibrium values (less fluctuation in R_g). For both low and neutral pH, R_g remains stable for most part of the simulation run, though there was much fall in the R_g value for high pH which also stabilizes after 12 ns of time.

A comparison between R_g values estimated in the present study for G5 PPI^{EDA} at different pH conditions and those for G5 PPI^{DAB} reported in the literature is presented in Table 4, which indeed shows that R_g values of G5 PPI^{EDA} (this work) and G5 PPI^{DAB} (our previous work)[66] are very similar. The calculated R_g value for G5 PPI^{EDA} dendrimer at high pH (12.73 ± 0.13 Å) is in reasonably good agreement with the available SAXS (14.30 Å)[88] and SANS (13.90 Å)[89] data for G5 PPI^{DAB} dendrimer. Moreover, the trend of R_g values obtained for G5 PPI^{EDA} (this work) and G5 PPI^{DAB} (our previous work)[66] from high to neutral pH is very similar to that of theoretical values reported by Wu.[90] It was interesting to observe that pH dependent swelling of the PPI dendrimer (increase in R_g values, Table 4) from high to low pH conditions is very similar to that reported for PAMAM dendrimer.[91] PPI dendrimers at high pH are non-protonated which allows compactness in the structure. At neutral and low pH dendrimer amines are protonated which results in a strong electrostatic repulsion making the structure very open, and hence more water can penetrate in the interior of the dendrimer structures. Instantaneous snapshots of the equilibrated dendrimer structure (after 20 ns) reflecting pH-induced conformation changes are depicted in Fig. 3.

Shape of dendrimers. The shape of the dendrimer is a significant property used widely for the characterization of its geometrical features. Theoretically, it can be assessed from the average values of the three principal moments of inertia I_x, I_y, I_z (in descending order). The ratio of the principal moments (I_x/I_y and I_x/I_z) *i.e.* aspect ratio can give a measure of shape in terms of spherical or ellipsoidal shape of the dendrimer. Moreover, asphericity (δ) values are also useful to analyze the shape of dendrimers and can be calculated by using the definition given by Rudnick and Gaspari[92] as:

$$\delta = 1 - 3\frac{\langle I_2 \rangle}{\langle I_1^2 \rangle}$$

where I_1 and I_2 are defined as $I_1 = I_x + I_y + I_z$ and $I_2 = I_xI_y + I_yI_z + I_xI_z$.

Aspect ratios and asphericity values for the G5 PPI^{EDA} and G5 PPI^{DAB} dendrimers at high, neutral and low pH are presented in Table 5. Comparison of the aspect ratio and asphericity values among the G5 PPI^{EDA} and G5 PPI^{DAB} dendrimers for the same pH indicates that the former is more spherical than the latter. It can be observed from the table that I_x/I_y and I_x/I_z values are in the order: high pH > neutral pH > low pH for both G5 PPI^{EDA} and G5 PPI^{DAB} dendrimers. This signifies that as we move from high to low pH, the shape of dendrimer adopts a more spherical geometry (average aspect ratio values are closer to unity). The snapshots for G5 PPI^{EDA} dendrimer (Fig. 3) also show that the equilibrated geometry of protonated dendrimer corresponding to neutral and low pH is more globular as compared to high pH. The reason behind this observation can be ascribed to the strong electrostatic repulsion between the protonated primary and tertiary amino groups in the case of neutral and low pH. As a result of which dendrimer arms get more stretched and it becomes spherical in nature. Moreover, protonated dendrimers have more surface area and can form favorable interaction with the solvent as compared to ellipsoidal shape geometries.[91]

Radial density distribution profiles. For better understanding the conformational behaviour of the PPI dendrimer at different

Table 4 Comparison of calculated radius of gyration R_g (Å) values for G5 PPI^{EDA} obtained in this work with the other reported theoretical and experimental results for G5 PPI^{DAB}

	This work (GAFF)[a]	GAFF[a] (ref. 66)	OPLS (ref. 90)	SANS (ref. 89)	SAXS (ref. 88)
pH	G5 PPI^{EDA}	G5 PPI^{DAB}	G5 PPI^{DAB}	G5 PPI^{DAB}	G5 PPI^{DAB}
High	12.73 ± 0.13	12.97 ± 0.19	12.34 ± 0.07	13.90	14.30
Neutral	15.77 ± 0.21	16.10 ± 0.16	15.99 ± 0.14	—	—
Low	16.29 ± 0.11	16.61 ± 0.11	15.83 ± 0.18	—	—

[a] Here R_g was averaged over the last 2 ns simulation run with each snapshot taken after 1 ps. The theoretical R_g values reported by Scherrenberg *et al.*[89] (CVFF) and Bodnar *et al.*[100] (PCFF) are 12.50 Å and 15.0 Å respectively.

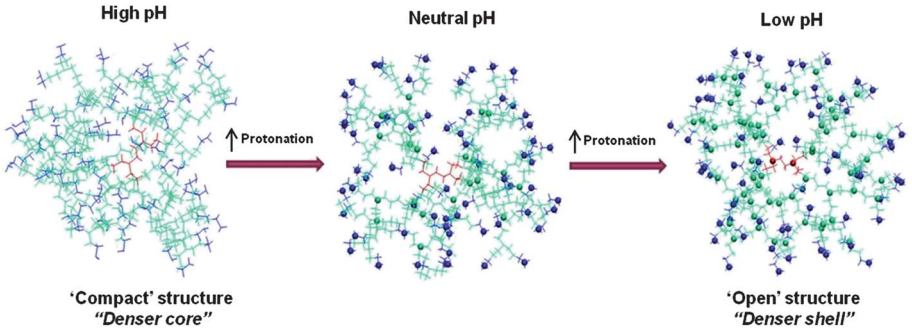

Fig. 3 pH-induced conformational changes in G5 PPI^{EDA} dendrimer (snapshots captured from the equilibrated geometry obtained after 20 ns simulation run). Colour coding for the line representation of dendrimers is as follows: red – core ('aaa'); green – repeating fragments ('bbb'); blue – terminal amino groups ('ccc'). Blue sphere – protonated primary amines, green sphere – protonated tertiary amines and red sphere – protonated tertiary amines of the core (only at low pH). Water and counterions are not shown for clarity and the dendrimers shown are rendered at scale relative to each other.

Table 5 Aspect ratios and asphericities for G5 PPI^{EDA} and G5 PPI^{DAB} dendrimers at high, neutral and low pH conditions

	Aspect ratio[a]				Asphericity[a] (δ)		
	G5 PPI^{EDA} (This work)		G5 PPI^{DAB} (ref. 66)		This work (GAFF)	GAFF (ref. 66)	OPLS (ref. 90)
pH	I_x/I_y	I_x/I_z	I_x/I_y	I_x/I_z	G5 PPI^{EDA}	G5 PPI^{DAB}	G5 PPI^{DAB}
High	1.21 ± 0.09	2.59 ± 0.18	1.53 ± 0.18	4.03 ± 0.41	0.0619	0.1172	0.0027
Neutral	1.21 ± 0.09	1.47 ± 0.12	1.35 ± 0.12	1.64 ± 0.12	0.0131	0.0219	0.0059
Low	1.14 ± 0.06	1.37 ± 0.11	1.25 ± 0.08	1.42 ± 0.11	0.0086	0.0115	0.0091

[a] Here properties were averaged over the last 2 ns simulation run with each snapshot taken after 1 ps.

pH conditions, radial density distribution, $\rho(r)$ profiles were also calculated. Fig. 4a illustrates the average radial monomer density profile with respect to the COM of the G5 PPI^{EDA} dendrimer at three different pH conditions. The density distribution in the dendrimer at high pH condition is greater as compared to neutral and low pH conditions, signifying a compact structure. The graph shows total density with two maxima and a minimum between them for all the pH. The first maximum for high pH condition is at 8 Å away from the core, whereas for neutral and low pH conditions it is close to 3 Å. The minimum is located at 10 Å and 6 Å away from the core for non-protonated (high pH) and protonated dendrimers (neutral/low pH) respectively. The second maximum density at high pH condition shifts from 12 Å to about 14 Å at low and neutral pH, and it is followed by a monotonic decay to the edge of the molecule. The trend of density profiles in the plot signifies that several cavities are present in the interior of the dendrimer, which is responsible for the high encapsulation efficiency of drug/guest molecules.

From Fig. 4a, the presence of a small constant density zone in G5 PPI^{EDA} dendrimer at all the three pH conditions can be seen but at different distances from the COM. For high pH it is ranging from 6–11 Å (close to the core) and for neutral as well as low pH conditions the value is in the range of 12–16 Å (close to the periphery). This is because at high pH condition dendrimer is non-protonated, thus resulted in a compact structure with "denser core", while at neutral and low pH conditions, dendrimers are protonated which leads to strong electrostatic repulsions and therefore "denser shell" (see Fig. 3). Another reason behind the greater mass distribution near the periphery of dendrimers at low and neutral pH could be attributed to the intramolecular hydrogen bonding within the dendrimer–water–counterions system, which results in the denser packing of the outer shell. In order to corroborate this possibility, initially we have quantitatively determined the number of hydrogen bonds formed between peripheral primary amines ('ccc' residue) of G5 PPI^{EDA} dendrimer and water molecules at different pH conditions (Fig. S6†). The plots signify that donor primary amines have a strong ability to form hydrogen bonds with the acceptor water molecules at all the three pH conditions. However, persistency of hydrogen bonds throughout the trajectory (last 2 ns of simulation run) at low and neutral pH conditions (protonated primary amines) is more in comparison to high pH condition (non-protonated primary amines).

Fig. 4b represents the radial density profile of water molecules around the center-of-mass of G5 PPI^{EDA} dendrimer at different pH conditions. The trends of density profiles of water at low and neutral pH are almost identical, and up to the distance of 14 Å from the COM the densities at these two pH conditions are much higher than that of the high pH condition. This difference can be explained by the pH induced conformational changes in G5 PPI^{EDA} dendrimer (Fig. 3), a more "open" structure is present at low and neutral pH conditions, which makes the dendrimer's interior more spacious as compared to the compact structure at high pH condition. Therefore, water molecules can easily penetrate in the interior

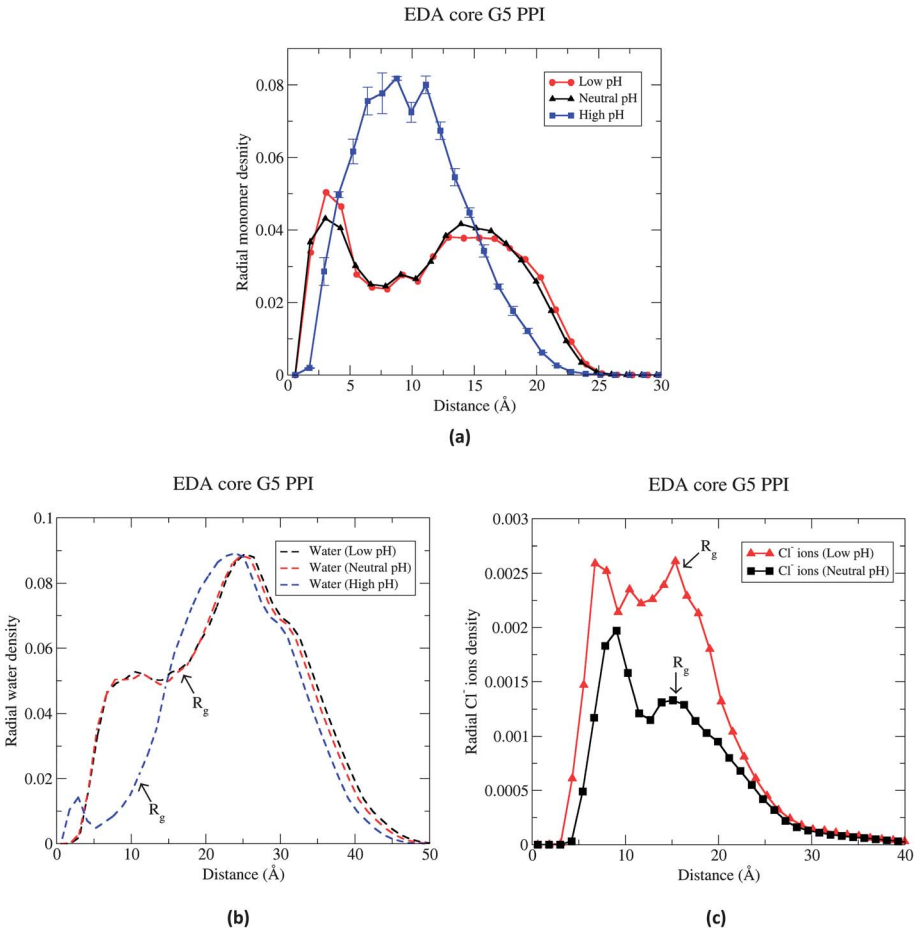

Fig. 4 Radial density ($\rho(r)$) distribution profiles around the center-of-mass for (a) G5 PPI^{EDA} dendrimer at all the three pH conditions (representative error bars are shown for the high pH case), (b) water at all the three pH conditions and (c) Cl^- counterions at low and neutral pH conditions. Density distribution was calculated for each snapshot saved at 1 ps interval over the last 2 ns run and then averaged.

of PPI dendrimer at low and neutral pH conditions. At distances close to 10 Å from the COM of dendrimer, a water density peak can be seen at low and neutral pH conditions, reflecting a large number of water molecules at this position. It can also be observed from the graphs that before reaching the bulk density of water, at the distances roughly corresponding to R_g of G5 PPI^{EDA} dendrimer at different pH conditions, there is a sharp increase in the density of water.

The density distribution for Cl^- counterions around the COM of G5 PPI^{EDA} dendrimer at low and neutral pH conditions is depicted in Fig. 4c, which clearly shows that ions have penetrated well in the interior of dendrimer. As expected, the density of counterions at low pH (fully protonated PPI dendrimer) is higher in comparison to neutral pH (2/3 protonated PPI dendrimer). Also, the graph illustrates that the trend of ion density distribution is different at both the pH. At low pH condition a small constant density zone is found from 10–15 Å, while at neutral pH condition instead of a constant density zone, a minimum is found close to 13 Å. This variation is again attributed to the different protonation level of G5 PPI^{EDA} dendrimer at low and neutral pH conditions. Nonetheless, in both the cases, a first maximum was found close to 10 Å, which might be due to the presence of high density of water at this position. The second maximum at both the pH conditions is present near the periphery of the dendrimer, indicating that Cl^- ions are close to the positively charged primary amines.[93]

The above analysis thus endorses the possibility that at low and neutral pH conditions protonated primary amines have the ability to form water and Cl^- ions (good density distribution near the periphery) mediated intramolecular hydrogen bonding ($Cl^-NH_3^+$–H_2O–$NH_3^+Cl^-$), which resulted in denser packing of the outer shell.

3.1.2 Stability of G5 PPI^{EDA}–Famo and G5 PPI^{EDA}–Indo complexes. To assess the extent of thermodynamic stability of the dendrimer–drug complexes (G5 PPI^{EDA}–Famo and G5 PPI^{EDA}–Indo) under different pH conditions, they were subjected to 6–10 ns MD simulations run. For the quantitative measurement of stability, the COM separation distance (Å) between G5 PPI^{EDA} dendrimer and drug molecules (Famo and Indo) during the whole simulation run was plotted as a function of time (ns) and is presented in Fig. 5. From the plot, it is apparent that at low pH, there is a steep increase in the COM distance and the drug molecules Famo and Indo move away from the dendrimer COM, thus indicating unstable

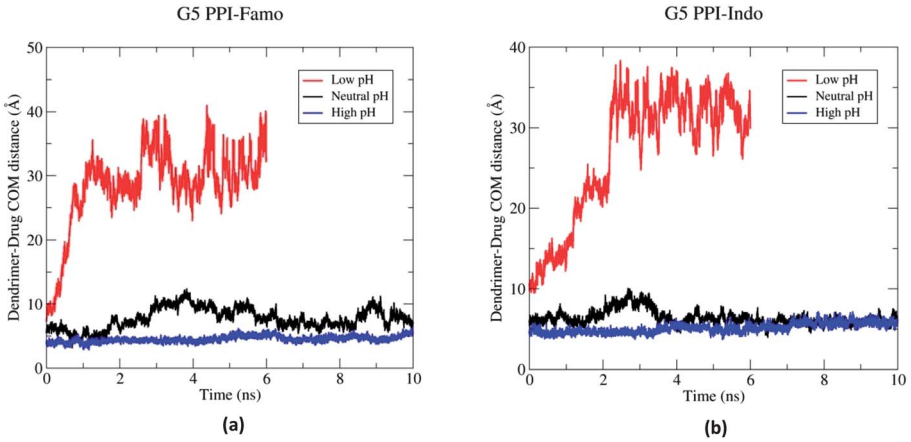

Fig. 5 Center-of-mass (COM) separation distance (Å) during the whole MD simulation run between (a) G5 PPI^{EDA} and Famo (b) G5 PPI^{EDA} and Indo.

complexation. In the case of G5 PPI^{EDA}–Famo at neutral pH, some fluctuations can be seen in the COM distance (reaching maximum up to 12 Å) but drug always remains within the dendrimer R_g (15.77 Å). In the case of G5 PPI^{EDA}–Indo at neutral pH, the COM distance touches the maximum value of 10 Å and most of the time it is fluctuating near 5 Å, indicating its close proximity with the dendrimer core. At high pH, the COM distance is constant (fluctuating near 5 Å) throughout the simulation in both the cases. This indicates that dendrimer–drug complexes are stable at neutral and high pH conditions. Snapshots of the G5 PPI^{EDA}–Famo and G5 PPI^{EDA}–Indo complexes at various pH conditions are presented in Fig. S7 and S8† respectively.

The above analysis implies that at low pH conditions, both the drug molecules (Famo and Indo) remain in uncomplexed form in the G5 PPI^{EDA} dendrimer solution, which is in qualitative agreement with the available experimental study where no significant increase in the solubility of Famo and Indo was observed *via* dendrimer at low pH.[35] In general, less solubility means less affinity for a drug or spontaneous release of a drug. Previous MD simulation studies reported for a PAMAM–Ibuprofen (a weakly acidic NSAID, pK_a = 4.5) complex at different pH conditions also found the unstable dendrimer–drug complex at low pH.[56] Moreover, earlier experimental studies on the solubility of acidic hydrophobes in PAMAM derivatives demonstrated that complexes remain stable at neutral pH conditions for a longer period of time, while they are unstable at low pH resulting in precipitate formation.[94,95] Likewise, Indo complexed with PAMAM dendrimer at physiologic/neutral pH conditions was also reported to be sufficiently stable and able to enhance the aqueous solubility of drug several times.[96]

To further substantiate our MD simulation analysis and to obtain better insight in the dendrimer–guest interactions, PMF calculations and binding free energy estimation using the MM-PBSA approach were also performed.

3.1.3 PMF calculations: Drug release and solubility profile of G5 PPI^{EDA}–Famo and G5 PPI^{EDA}–Indo complexes. PMF plots for the six cases (G5 PPI^{EDA} with Famo and Indo at low, neutral and high pH) are shown in Fig. 6. Each PMF curve represents the free energy barrier for the release of drug molecules from the dendrimer cavity at different pH conditions. Fig. 6 clearly shows that at low pH conditions the release of the drugs is spontaneous, since no net energy barrier is noticeable; continuous decrease in PMF values recorded as a function of increasing distance. This observation is in agreement with our MD simulation results at low pH conditions, where drugs (Famo and Indo) move away from the G5 PPI^{EDA} dendrimer during the course of simulation. At neutral pH condition there is a shallow potential well along the drug release path, indicating some stability to the dendrimer–drug complexes. At high pH conditions the minimum of the PMF is very deep indicating the strong dendrimer–drug interactions as well as a very slow drug

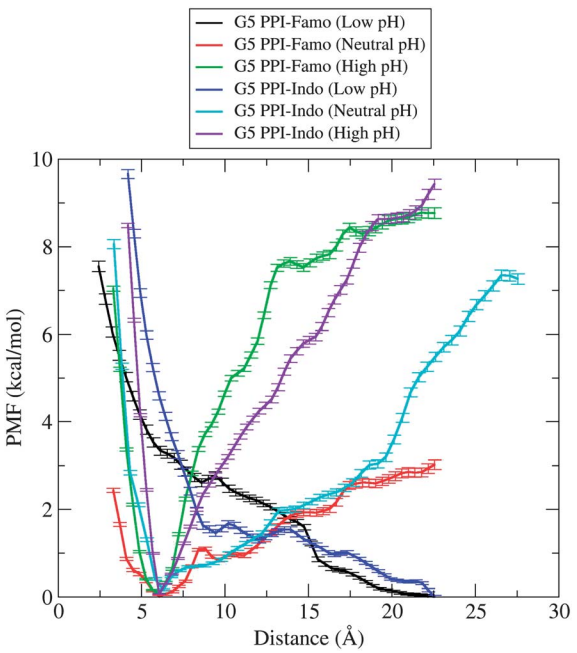

Fig. 6 PMF plot (with error bars) for Famo and Indo drug molecules bound with G5 PPI^{EDA} dendrimer at all the three pH conditions.

release profile. The free energy barrier calculated for G5 PPI^{EDA}–Famo at neutral pH and high pH was found to be about 3.0 kcal mol^{-1} and 8.8 kcal mol^{-1} respectively; whereas for G5 PPI^{EDA}–Indo at neutral and high pH it was found to be about 7.4 kcal mol^{-1} and 9.4 kcal mol^{-1} respectively.

The PMF profiles also show that the difference in the free energy barrier calculated for G5 PPI^{EDA}–Famo (3.0 kcal mol^{-1}) and G5 PPI^{EDA}–Indo (7.4 kcal mol^{-1}) complexes at neutral pH is quite substantial. This difference can be attributed to the fact that at neutral pH, Indo exists in anionic form which can make strong electrostatic interactions with the positively charged dendrimer, while Famo exists in neutral state thus the possibility of such interactions is ruled out. On the other hand, at high pH conditions the PMF energy barrier for both the complexes (G5 PPI^{EDA}–Famo and G5 PPI^{EDA}–Indo) is almost the same; since in this case dendrimer is non-protonated and hydrophobic drugs (Famo and Indo) can bind to it through strong nonpolar hydrophobic or van der Waals interactions, rather than electrostatic interactions.

Why is the low pH environment not good for drug solubility or in other words gives rise to the unstable drug–dendrimer complex? At low pH tertiary as well as primary amines of PPI dendrimer are fully protonated, resulting in an extremely polar environment and an "open" conformational state of dendrimer as revealed from Fig. 3. This conformation of dendrimer arises due to electrostatic repulsions and might not be able to firmly hold the drug molecules, ensuing in a brisk release. In addition, at low pH Famo exists in cationic form (ionized), thus it is expected to experience strong electrostatic repulsions and in effect a large amount of destabilization is produced in the system. Whereas, Indo exists in neutral state (unionized) at low pH, which is quite hydrophobic in nature, hence forming an unstable complex with the host molecule. In general, it can be said that the persistent decrease in PMF values with increase in the distance represents highly unfavorable encapsulation of the ligand.

In the experimental study,[35] only phase solubility studies were performed for G5 PPI^{EDA}–Famo and G5 PPI^{EDA}–Indo at different pH conditions and no release profile was reported, thus to validate our PMF calculations based suggested release profile we thoroughly searched for the alternative literature. In line with our observation, a similar trend of release profile at different pH conditions (low pH – triggered simultaneous release; neutral pH – medially sustained release; high pH – enormously slower release) was also reported experimentally for anti-leukaemic drugs methotrexate and all-*trans* retinoic acid from the G4 PAMAM dendrimer–drugs complex.[97] Moreover, experimental studies carried out by Devarakonda *et al.*[98] also suggest that at low pH the PAMAM dendrimer releases the hydrophobic drug Furosemide (loop diuretic anti-hypertensive) at a very fast rate in comparison to neutral pH. In another study, Pistolis *et al.*[99] explored the potential of PPI dendrimer as a pH sensitive controlled release system and found that the expulsion of pyrene is induced at low pH.

Besides the release profile of drug molecules from the dendritic matrix, the PMF plot can also be interpreted in other way *i.e.* in terms of pH suitable for the ease of drug loading in host dendrimer and thus the corresponding solubility. A high PMF barrier for a particular dendrimer–drug complex signifies that dendrimer has good ability to strongly hold the drug molecule. In the present study, the energy barrier for G5 PPI^{EDA}–Famo (8.8 kcal mol^{-1}) and G5 PPI^{EDA}–Indo (9.4 kcal mol^{-1}) is highest at high pH conditions and negligible at low pH conditions. Thus accordingly, maximum and minimum drug loading (Famo and Indo) in G5 PPI^{EDA} dendrimer is suggested to be at high and low pH conditions respectively. Moreover, solubilization is an associative mechanism driven by thermodynamics of the dendrimer–drug complex, the trends of the PMF free energy barrier obtained can be directly correlated with the trends of solubilization enhancement at different pH conditions. Therefore, from the analysis of PMF plot (Fig. 6) the order of solubilization enhancement for G5 PPI^{EDA}–Famo and G5 PPI^{EDA}–Indo complexes is proposed to be high pH > neutral pH > low pH, which is in good agreement with the pertinent experimental study.[35] This comparison helps to validate the theoretical results and methodologies reported in this article which can be extended further to study similar phenomena in other dendrimer–drug complexes.

3.1.4 MM-PBSA calculations to analyze energy contributions for G5 PPI^{EDA}–Famo and G5 PPI^{EDA}–Indo complexes. In addition to PMF calculations, binding free energy was also estimated at each umbrella window using the MM-PBSA approach for G5 PPI^{EDA}–Famo (Fig. 7) and G5 PPI^{EDA}–Indo (Fig. S9†) complexes at low, neutral and high pH conditions. These plots show that the overall binding free energy (PBTOT) has fluctuations along each window, which may be attributed to the fact that dendrimer consists of several pockets with different chemical environments, and hence different binding energy patterns can be obtained as one drags the ligand inside (push) or outside (pull) the dendrimer. The trend of PBTOT for G5 PPI^{EDA}–Famo was found to be high pH > neutral pH > low pH (Fig. 7). It can be revealed from the plot that at low pH (Fig. 7a) the G5 PPI^{EDA}–Famo complex is thermodynamically unstable, since the binding free energy values are positive, reflecting unfavorable binding. While negative values of PBTOT at neutral (Fig. 7b) and high pH (Fig. 7c) signify favorable binding (exothermic). This observation is in accordance with the findings of the MD simulations and PMF analysis of the G5 PPI^{EDA}–Famo complex.

In order to understand the driving forces behind the encapsulation, various components of the overall binding free energy at each umbrella window were also calculated. PBTOT can be decomposed into two major components (i) PBELE (sum of the electrostatic solvation free energy and MM electrostatic energy) and (ii) PBNP (sum of the nonpolar solvation free energy and MM van der Waals energy). At low pH conditions (Fig. 7a), the trend of variation of PBELE is similar to the PBTOT for the G5 PPI^{EDA}–Famo complex. Thus, it is the unfavorable electrostatic interactions playing a major role in making the G5 PPI^{EDA}–Famo complex unstable at low pH conditions. The MM-PBSA plot of the G5 PPI^{EDA}–Famo complex at neutral (Fig. 7b) and high pH (Fig. 7c) conditions illustrates a similar quantitative trend for PBELE. While, clear differences can be seen in the PBNP at these two pH conditions. This signifies that PBNP is

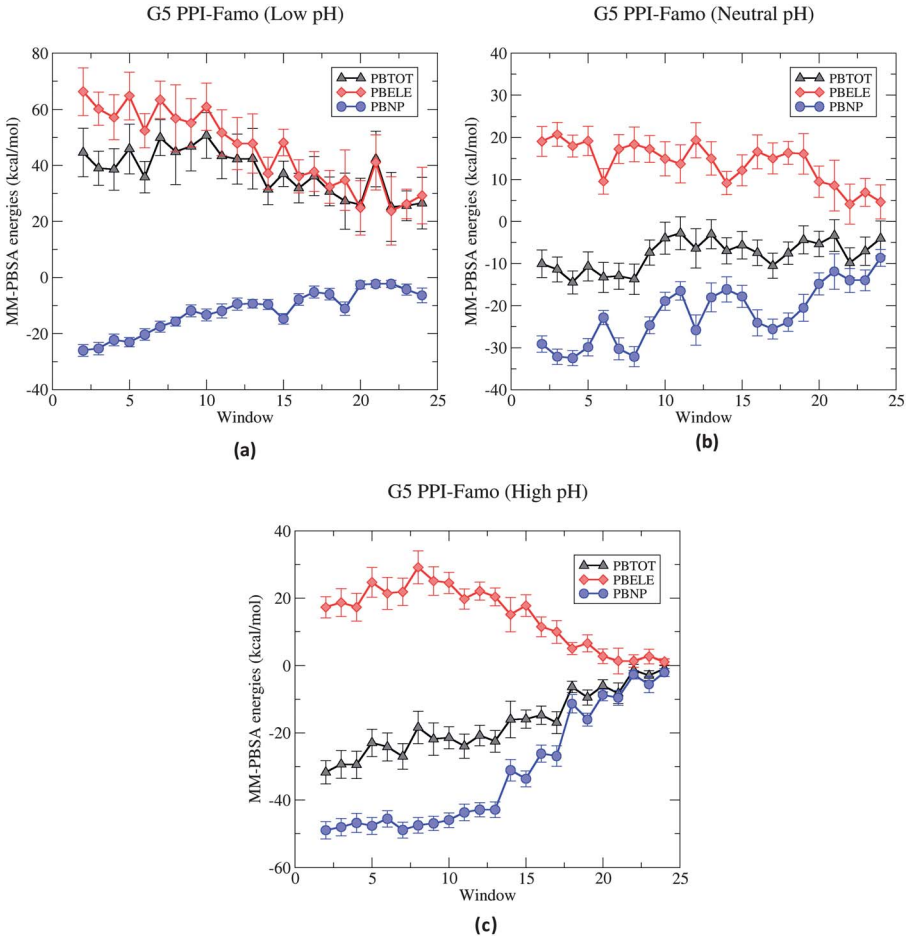

Fig. 7 Plots (with Std. Dev. bars) showing different energy components of MM-PBSA for the G5 PPI^{EDA}–Famo complex at (a) low pH, (b) neutral pH and (c) high pH. PBTOT = PBELE + PBNP; abbreviations: PBTOT = final estimated binding free energy, PBELE = electrostatic solvation free energy (PBCAL) + MM electrostatic energy (ELE), PBNP = nonpolar solvation free energy (PBSUR) + MM van der Waals energy (VDW).

playing a pivotal role in making the G5 PPI^{EDA}–Famo complex stable at high pH (higher PBTOT and PBNP as compared to neutral pH). This is because at high pH the nonpolar environment of the dendrimer is able to make good van der Waals interactions with the hydrophobic drug molecule Famo.

Furthermore, specific intermolecular interactions *viz.* hydrogen bonding between drug molecule Famo and G5 PPI^{EDA} dendrimer at different pH conditions for each umbrella sampling window were also explored (Fig. 8). In particular, hydrogen bond acceptors and donors of both the side chains of Famo *i.e.* *N*′-sulfamoylpropanamidine and guanidine were found to be involved in hydrogen bonding formation with the primary and tertiary amines of G5 PPI^{EDA} dendrimer. Fig. 8 shows that the hydrogen bond forming ability of Famo with the dendrimer is in the order of high pH > neutral pH > low pH, in accordance with the trend of MM-PBSA binding free energy and PMF calculated free energy barrier. This implies that the propensity of hydrogen bonding of Famo with G5 PPI^{EDA} is more in the case of compact dendrimer structures as compared to the "open" structure. Thus, hydrogen bonding plays an important role in making the dendrimer–drug complex stable and also contributes significantly in raising the free energy barrier.

The energetic contribution by various components to the overall binding free energy at each umbrella window was also plotted for the G5 PPI^{EDA}–Indo complex at all the three pH

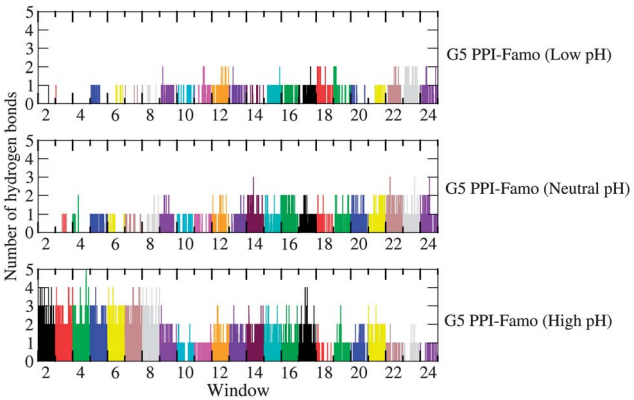

Fig. 8 Plots showing hydrogen bonds formation ability of drug molecule Famo (*N*′-sulfamoylpropanamidine and guanidine moiety) with the G5 PPI^{EDA} dendrimer (primary and tertiary amino groups) at low, neutral and high pH conditions. *X* axis represents the umbrella sampling window (each 1 ns simulation run and hydrogen bonds were calculated on each snapshot after 1 ps). For calculating hydrogen bonds, angle and distance cutoff was set to 120° and 3.0 Å respectively.

conditions (Fig. S9†). Here, the trend of PBTOT was found to be neutral pH > high pH > low pH. In similar line with the G5 PPI^{EDA}–Famo, here also it can be observed that the G5 PPI^{EDA}–Indo complex at low pH conditions (Fig. S9a†) is thermodynamically unstable (PBTOT fluctuating near zero). This can be attributed to the unfavorable PBELE that is positive throughout the windows. At neutral (Fig. S9b†) and high pH (Fig. S9c†), negative values of PBTOT for the G5 PPI^{EDA}–Indo complex indicate favorable binding (exothermic reaction), which is consistent with the MD simulations and PMF analysis. At neutral pH conditions (Fig. S9b†) PBELE and PBNP both are favorable (negative values). While at high pH conditions (Fig. S9c†), PBELE is unfavorable (positive values) and PBNP is favorable (negative values). At neutral pH conditions Indo (anionic) can be associated with the PPI dendrimer *via* two mechanisms, encapsulation in the cavity of dendrimer *via* van der Waals interactions and secondly electrostatic interactions with the positively charged amines. Conversely, at high pH only the former interactions are possible which can be responsible for the encapsulation.

Here also, the hydrogen bond formation ability of Indo with G5 PPI^{EDA} dendrimer at different pH conditions for each umbrella sampling window (Fig. S10†) was found to be in agreement with the MM-PBSA binding free energy trend *i.e.* neutral pH > high pH > low pH. The reason being, only at neutral pH condition the carboxylic acid group of Indo is deprotonated which has a strong ability to form hydrogen bonding with the protonated primary and tertiary amines of G5 PPI^{EDA} dendrimer.

3.2 Influence of chemical environment of dendrimers (G3 PAMAM and G4 PPI^{DAB}) on the release and solubility profile of Pbz

The solubility and release profile of the guest molecule from the dendrimer gets modulated as a function of the chemical environment provided by the host. The protocol established in the previous section can be utilized for distinguishing the differences in the influence of chemical environment of dendrimer on the drug solubility and release profile. To establish the same, we have considered the experimental study where the differences are reported for the aqueous solubility and release profile of drug Pbz in G3 PAMAM and G4 PPI^{DAB} dendrimers.[44] The internal structure of PAMAM consists of amido groups, alkyl chain and tertiary amines, while PPI composed of alkyl chain and tertiary amines. Moreover, the length of branching units for PAMAM and PPI dendrimers is 7 and 4 bonds respectively, indicating that the size of PAMAM dendrimer is much larger as compared to PPI dendrimer with an equivalent number of peripheral amines (32 surface groups).

To understand the thermodynamic stability of G3 PAMAM–Pbz and G4 PPI^{DAB}–Pbz complexes at neutral pH, the complexes were simulated for several ns. The COM distance (Å) between the dendrimers and drug molecule as a function of time (ns) is shown in Fig. 9. It is clearly reflected from the figure that drug molecule Pbz binds tightly with both the dendrimers at neutral pH conditions, and therefore forming stable complexation.

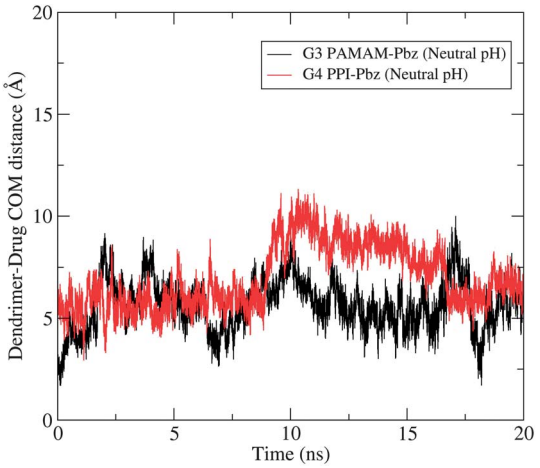

Fig. 9 Center-of-mass (COM) separation distance (Å) between the drug Pbz and dendrimers (G3 PAMAM and G4 PPI^{DAB}) during the 20 ns MD simulation run at neutral pH conditions.

PMF calculations were carried out at neutral pH to estimate the free energy barrier for Pbz complexed with two different dendrimers (G3 PAMAM and G4 PPI^{DAB}) and plotted as a function of distance (Fig. 10). The PMF plot indicates that drug molecule Pbz experiences a higher free energy barrier (about 8.6 kcal mol^{-1}) to get released from G3 PAMAM. The free energy barrier for the release of Pbz from G4 PPI^{DAB} is only about 1.1 kcal mol^{-1}. This implies that the G3 PAMAM–Pbz complex might show sustained release behavior in contrast to fast release from the G4 PPI^{DAB}–Pbz complex at a physiological pH (~7.4). This observation is in good agreement with the relevant experimental results, where only 13% of the drug was found in the outer phase of the dialysis bag after 12 h for G3 PAMAM, whereas in the same period 44% of the drug gets released from the G4 PPI^{DAB}–drug complex.[44]

Since a high PMF energy barrier signifies tight binding between dendrimer and drug, the following order can be proposed on the basis of the PMF plot (Fig. 10) for the solubility

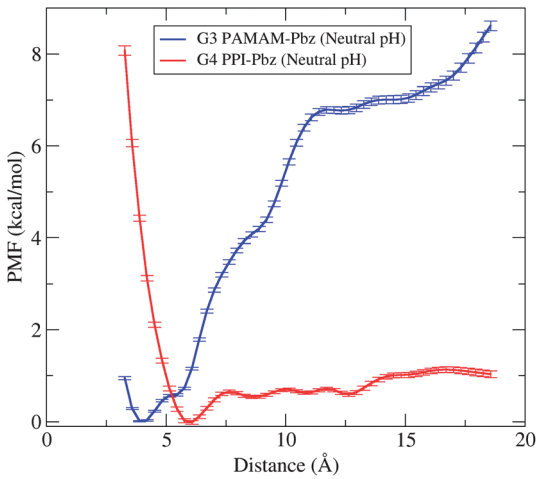

Fig. 10 PMF plot (with error bars) for Pbz drug molecule bound with G3 PAMAM and G4 PPI^{DAB} at neutral pH conditions.

enhancement of drug Pbz at neutral pH, G3 PAMAM > G4 PPI^{DAB}. This is again in accordance with the experimental results,[44] where the solubility of Pbz was found to be increasing linearly with an increase in the G3 PAMAM dendrimer concentration. Conversely, an increase in the concentration of G4 PPI^{DAB} dendrimer rarely enhances Pbz solubilization. An equilibrium snapshot of G3 PAMAM–Pbz and G4 PPI^{DAB}–Pbz complexes corresponding to minimum PMF values is illustrated in Fig. 11. From the figure, differences in the structure and shape of the G3 PAMAM (compact, spherical) and G4 PPI^{DAB} (hollow, ellipsoidal) dendrimers can be clearly seen, which arises due to the different internal chemical environment and level of protonation in the G3 PAMAM (only primary amines protonated – 32 positive charge) and G4 PPI^{DAB} (2/3 protonation – 42 positive charge).

Binding free energy estimations using MM-PBSA at each umbrella window for G3 PAMAM–Pbz and G4 PPI^{DAB}–Pbz complexes (Fig. 12) demonstrated that the former complex is more thermodynamically stable (overall higher binding free energy-PBTOT) compared to the latter. The contribution of different components to the overall binding free energy at each umbrella window for G3 PAMAM–Pbz and G4 PPI^{DAB}–Pbz (neutral pH) complexes is also depicted in Fig. 12. The trends in the variation for the binding free energy (PBTOT) are entirely reflected in the total nonpolar contribution (PBNP) for both the cases, thus it can be inferred that van der Waals interaction of Pbz with the dendrimer pockets is the primary mechanism of encapsulation. Although, anionic Pbz can interact with cationic dendrimers through ionic interactions, but the overall electrostatic contribution (PBELE) in the case of G3 PAMAM is unfavorable whereas it is favorable in the case of G4 PPI^{DAB}. At high pH, G3 PAMAM and G4 PPI^{DAB} only differ in the internal environment where the former is quite hydrophilic in nature (consists of polar amide groups) and the latter is hydrophobic (consists of nonpolar alkyl chains). However, at neutral pH conditions in addition to the internal chemical environment, the protonation level of amines in both the dendrimers is entirely different (PAMAM – only surface amines protonated, PPI – 2/3 amines protonated). This difference in the ionization state at neutral pH makes the PPI environment considerably

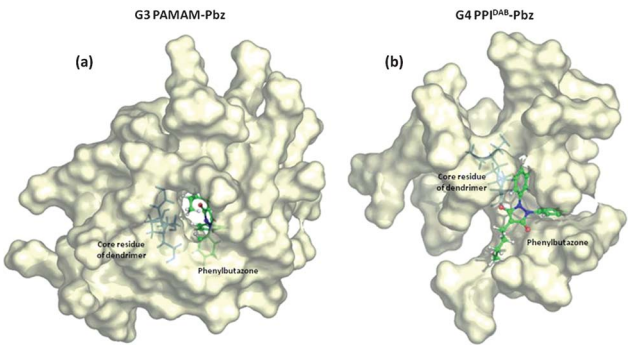

Fig. 11 Equilibrium snapshot of dendrimer–drug complexes at minimum PMF values. (a) G3 PAMAM–Pbz dendrimer (COM separation distance – 4.36 Å) (b) G4 PPI^{DAB}–Pbz dendrimer (COM separation distance – 6.26 Å). The dendrimers shown are rendered at scale relative to each other.

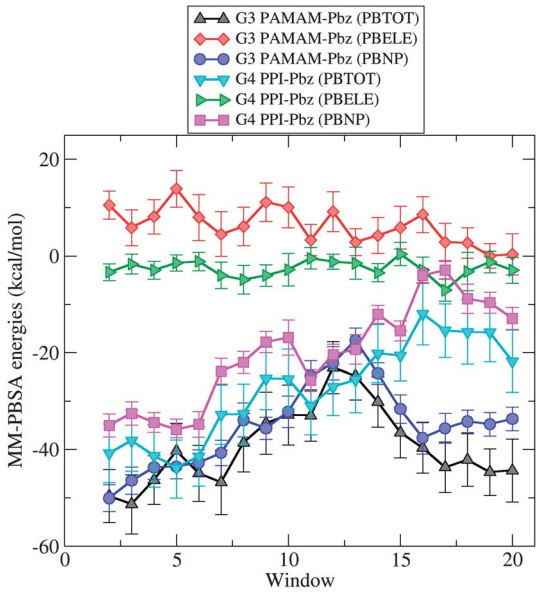

Fig. 12 Plot (with Std. Dev. bars) showing different energy components of MM-PBSA for G3 PAMAM–Pbz and G4 PPI^{DAB}–Pbz complexes at neutral pH. PBTOT = PBELE + PBNP; abbreviations: PBTOT = final estimated binding free energy, PBELE = electrostatic solvation free energy (PBCAL) + MM electrostatic energy (ELE), PBNP = nonpolar solvation free energy (PBSUR) + MM van der Waals energy (VDW).

polar as compared to PAMAM. This is why higher electrostatic and lower nonpolar contribution was observed for G4 PPI^{DAB}–Pbz in comparison to G3 PAMAM–Pbz.

Intermolecular hydrogen bond analyses for G3 PAMAM–Pbz and G4 PPI^{DAB}–Pbz at neutral pH conditions for each umbrella sampling window are presented in Fig. 13. Both the carbonyl oxygens at the pyrazolidine ring of Pbz were found to participate in hydrogen bonding interactions with the amide NH and protonated primary amines in the case of G3 PAMAM, whereas in the case of G4 PPI^{DAB} protonated primary and tertiary amines were involved in the intermolecular interactions. Hydrogen bond profiles shown in Fig. 13 clearly distinguish the hydrogen

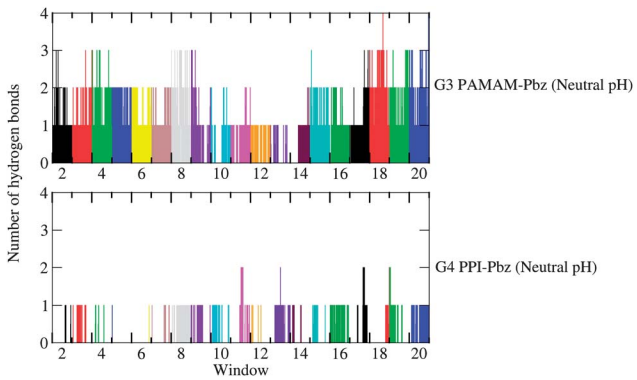

Fig. 13 Plots showing hydrogen bonds formation ability of drug molecule Pbz (carbonyl groups) with the EDA cored G3 PAMAM (amide and primary amino groups) and G4 PPI^{DAB} (primary and tertiary amino groups) dendrimers at neutral pH condition. *X* axis represents the umbrella sampling window (each 1 ns simulation run and hydrogen bonds were calculated on each snapshot after 1 ps). For calculating hydrogen bonds, angle and distance cutoff was set to 120° and 3.0 Å respectively.

bond formation ability of the drug molecule with the two different dendrimers and it was found in the order G3 PAMAM–Pbz > G4 PPI^{DAB}–Pbz. In addition to hydrophobic interactions, it is noteworthy that intermolecular hydrogen bonding provides extra stability to the dendrimer–drug complex and is one of the imperative mechanisms for ligand encapsulation. Moreover, from this analysis it was also found that intermolecular hydrogen bonds also contribute significantly in raising the free energy barrier.

In the experimental studies,[44] authors have considered only the differences in the chemistry of internal branching units of PAMAM and PPI dendrimers to be the primary reason behind the variability in the aqueous solubility and release. But, the present MD simulation study reveals that in addition to the structural differences, ionization states of the host dendrimer have significant implication in deciding the stability of complexation. Along with the above obtained results it can be concluded that theoretical studies can be successfully implemented to study host–guest interactions at the molecular level. The results interpreted could be extended to explain the phenomena like effect of pH, hydrophobes (pK_a, functional groups) and dendrimer chemistry on the drug loading, solubility and release.

4 Conclusions

In the present study, theoretical approaches such as MD simulations, PMF calculations and binding free energy analysis using the MM-PBSA method have been implemented to understand the solubility and release profile of hydrophobes with the dendrimers of different architecture at different pH conditions. Structural properties such as size, shape and density profile were calculated under various pH conditions (low, neutral and high). The size of the dendrimer was found to increase from high to low pH reflecting swelling due to the electrostatic phenomenon, a trend observed very similar to that of the PAMAM dendrimer. The results obtained for the radius of gyration values were found to be in agreement with the available theoretical and experimental results for the PPI dendrimer. Asphericity values and aspect ratio indicate that the shape of the dendrimer is more spherical at neutral and low pH conditions compared to the shape at high pH. The radial monomer density distribution profile of G5 PPI^{EDA} dendrimer suggested that several cavities are present at neutral and low pH where the structure is characterized by "denser-shell", while at high pH the structure is quite compact with "denser-core". Moreover at low and neutral pH conditions, high extent of hydrogen bonding between peripheral primary amines of G5 PPI^{EDA} dendrimer and water molecules, and substantial density distribution of water and Cl^- counterions near the periphery of dendrimer corroborate the possibility of intramolecular hydrogen bonding within the dendrimer–water–counterions system.

MD simulation analysis of the G5 PPI^{EDA}–Famo and G5 PPI^{EDA}–Indo complexes revealed that at low pH, the drug is present mostly in a free form without making complexation with the dendrimer. This might be a reason behind the low solubility of drugs at low pH conditions as observed during relevant experiments. To garner further support for this observation, a more rigorous approach based on PMF calculations was carried out to obtain the energy barrier for the release of drug molecule from the dendrimer cavity at different pH conditions. The results of this analysis signify spontaneous release of drug molecules at low pH, intermediate release at neutral pH and slow release at high pH. Moreover, this analysis also suggested that the solubilization enhancement for G5 PPI^{EDA}–Famo and G5 PPI^{EDA}–Indo complexes should adopt the following trend: high pH > neutral pH > low pH. Binding free energy calculations at each umbrella window using the MM-PBSA methodology further revealed the role of different non-bonded interaction energies in the stabilization/destabilization of the complex and thus in identifying the driving force behind the encapsulation.

Apart from gaining insight into the role of pH in the solubility and release profile of Famo and Indo with G5 PPI^{EDA} dendrimer, we have also tried to provide a microscopic origin for the differences in the aqueous solubility and release profile of Pbz drug complexed with G3 PAMAM and G4 PPI^{DAB} dendrimers. At neutral pH, the PMF study reveals slower release of Pbz from the G3 PAMAM as compared to G4 PPI^{DAB} dendrimer. PMF calculations also suggested the solubility trend at neutral pH as G3 PAMAM–Pbz > G4 PPI^{DAB}–Pbz, in accordance with the experimental observations. MM-PBSA analysis indicates that the favourable nonpolar interactions (van der Waals) between dendrimer and drug play a major role in the encapsulation. While, hydrogen bonding analysis showed that these intermolecular interactions also contribute significantly in the stabilization of dendrimer–drug complexes and raising the free energy barrier. Thus, this comprehensive study presents additional insight (i) in understanding the release as well as solubility profile of drugs with dendrimer at different pH and chemical environmental conditions, and (ii) in elucidating the mechanism of dendrimer–drug interactions. This computational protocol could assist the pharmaceutical scientist in better understanding the dendrimer–guest system in order to rationally design and optimize nano-formulation.

Conflict of interest

The authors declare no competing financial interest.

Acknowledgements

We are grateful to the Department of Science and Technology (DST), Nano mission, Delhi, Council of Scientific and Industrial Research (CSIR), Delhi and NIPER, S.A.S. Nagar, India for providing financial support. We are also thankful to the referees for giving their valuable comments/suggestions for the improvement of manuscript.

References

1 S. Kim, K. Kwon, I. C. Kwon and K. Park, in *Nanotechnology in Drug Delivery*, ed. M. D. V. Melgardt, P. Aramwit and

G. S. Kwon, Springer Science, New York, 2009, vol. X, Part IV, pp. 581–596.
2 A. R. Menjoge, R. M. Kannan and D. A. Tomalia, *Drug Discovery Today*, 2010, **15**, 171–185.
3 M. A. Mintzer and M. W. Grinstaff, *Chem. Soc. Rev.*, 2010, **40**, 173–190.
4 W.-d. Tian and Y.-q. Ma, *Chem. Soc. Rev.*, 2013, **42**, 705–727.
5 A. W. Bosman, H. M. Janssen and E. W. Meijer, *Chem. Rev.*, 1999, **99**, 1665–1688.
6 D. A. Tomalia, *Prog. Polym. Sci.*, 2005, **30**, 294–324.
7 U. Boas and P. M. H. Heegaard, *Chem. Soc. Rev.*, 2004, **33**, 43–63.
8 R. K. Tekade, P. V. Kumar and N. K. Jain, *Chem. Rev.*, 2008, **109**, 49–87.
9 V. Vasumathi and P. K. Maiti, *Macromolecules*, 2010, **43**, 8264–8274.
10 B. Nandy and P. K. Maiti, *J. Phys. Chem. B*, 2011, **115**, 217–230.
11 C. Dufes, I. F. Uchegbu and A. G. Schatzlein, *Adv. Drug Delivery Rev.*, 2005, **57**, 2177–2202.
12 V. A. Kabanov, A. B. Zezin, V. B. Rogacheva, Z. G. Gulyaeva, M. F. Zansochova, J. G. H. Joosten and J. Brackman, *Macromolecules*, 1998, **31**, 5142–5144.
13 P. K. Maiti and B. Bagchi, *Nano Lett.*, 2006, **6**, 2478–2485.
14 B. Nandy, M. Santosh and P. K. Maiti, *J. Biosci.*, 2012, **37**, 457–474.
15 Y. Cheng, L. Zhao, Y. Li and T. Xu, *Chem. Soc. Rev.*, 2011, **40**, 2673–2703.
16 J. N. H. Reek, S. Arevalo, R. van Heerbeek, P. C. J. Kamer and P. Van Leeuwen, *Adv. Catal.*, 2006, **49**, 71–151.
17 D. A. Tomalia, H. Baker, J. Dewald, M. Hall, G. Kallos, S. Martin, J. Roeck, J. Ryder and P. Smith, *Polym. J.*, 1985, **17**, 117–132.
18 E. M. M. de Brabander-van den Berg and E. W. Meijer, *Angew. Chem., Int. Ed. Engl.*, 1993, **32**, 1308–1311.
19 G. Jayamurugan and N. Jayaraman, *Tetrahedron*, 2006, **62**, 9582–9588.
20 C. Jana, G. Jayamurugan, R. Ganapathy, P. K. Maiti, N. Jayaraman and A. K. Sood, *J. Chem. Phys.*, 2006, **124**, 204719.
21 U. Gupta, H. B. Agashe, A. Asthana and N. K. Jain, *Biomacromolecules*, 2006, **7**, 649–658.
22 S. Svenson and A. S. Chauhan, *Nanomedicine*, 2008, **3**, 679–702.
23 C. Zhao, Y. Wang, Y. Su, H. Zhang, L. Ding, X. Yan, D. Zhao, N. Shao, X. Ye and Y. Cheng, *Int. J. Pharm.*, 2011, **421**, 301–319.
24 M. Na, C. Yiyun, X. Tongwen, D. Yang, W. Xiaomin, L. Zhenwei, C. Zhichao, H. Guanyi, S. Yunyu and W. Longping, *Eur. J. Med. Chem.*, 2006, **41**, 670–674.
25 A. K. Patri, J. F. Kukowska-Latallo and J. R. Baker, *Adv. Drug Delivery Rev.*, 2005, **57**, 2203–2214.
26 A. V. Ambade, E. N. Savariar and S. Thayumanavan, *Mol. Pharm.*, 2005, **2**, 264–272.
27 S. Svenson, *Eur. J. Pharm. Biopharm.*, 2009, **71**, 445–462.
28 G. L. Amidon, H. Lennernas, V. P. Shah and J. R. Crison, *Pharm. Res.*, 1995, **12**, 413–420.
29 A. D'Emanuele and D. Attwood, *Adv. Drug Delivery Rev.*, 2005, **57**, 2147–2162.
30 M. Liu, K. Kono and J. M. J. Frechet, *J. Controlled Release*, 2000, **65**, 121–131.
31 C. J. Hawker, K. L. Wooley and J. M. J. Frachet, *J. Chem. Soc., Perkin Trans. 1*, 1993, 1287–1297.
32 N. K. Jain and U. Gupta, *Expert Opin. Drug Metab. Toxicol.*, 2008, **4**, 1035–1052.
33 B. Devarakonda, R. A. Hill and M. M. de Villiers, *Int. J. Pharm.*, 2004, **284**, 133–140.
34 C. Yiyun and X. Tongwen, *Eur. J. Med. Chem.*, 2005, **40**, 1188–1192.
35 U. Gupta, H. B. Agashe and N. K. Jain, *J. Pharm. Pharm. Sci.*, 2007, **10**, 358–367.
36 R. N. Prajapati, R. K. Tekade, U. Gupta, V. Gajbhiye and N. K. Jain, *Mol. Pharm.*, 2009, **6**, 940–950.
37 L. Zhao, Q. Wu, Y. Cheng, J. Zhang, J. Wu and T. Xu, *J. Am. Chem. Soc.*, 2010, **132**, 13182–13184.
38 J. Hu, Y. Cheng, Q. Wu, L. Zhao and T. Xu, *J. Phys. Chem. B*, 2009, **113**, 10650–10659.
39 Y. Cheng, Q. Wu, Y. Li and T. Xu, *J. Phys. Chem. B*, 2008, **112**, 8884–8890.
40 W. Yang, Y. Li, Y. Cheng, Q. Wu, L. Wen and T. Xu, *J. Pharm. Sci.*, 2009, **98**, 1075–1085.
41 N. K. Jain, R. N. Prajapati, A. Agarwal, U. Gupta and A. Asthana, *Asian J. Pharm.*, 2009, **3**, 188–196.
42 D. Kannaiyan and T. Imae, *Langmuir*, 2009, **25**, 5282–5285.
43 E. Boisselier, L. Liang, M. Dalko-Csiba, J. Ruiz and D. Astruc, *Chem.–Eur. J.*, 2010, **16**, 6056–6068.
44 N. Shao, Y. Su, J. Hu, J. Zhang, H. Zhang and Y. Cheng, *Int. J. Nanomed.*, 2011, **6**, 3361–3372.
45 Y. Haba, A. Harada, T. Takagishi and K. Kono, *J. Am. Chem. Soc.*, 2004, **126**, 12760–12761.
46 D. L. Richter-Egger, A. Tesfai and S. A. Tucker, *Anal. Chem.*, 2001, **73**, 5743–5751.
47 P. Miklis, T. Cagin and W. A. Goddard III, *J. Am. Chem. Soc.*, 1997, **119**, 7458–7462.
48 P. Posocco, M. Ferrone, M. Fermeglia and S. Pricl, *Macromolecules*, 2007, **40**, 2257–2266.
49 F. Avila-Salas, C. Sandoval, J. Caballero, S. Guiñez-Molinos, L. S. Santos, R. E. Cachau and F. D. González-Nilo, *J. Phys. Chem. B*, 2012, **116**, 2031–2039.
50 T. Lewis and V. Ganesan, *J. Phys. Chem. B*, 2012, **116**, 8269–8281.
51 T. Lewis and V. Ganesan, *Soft Matter*, 2012, **8**, 11817–11830.
52 V. Maingi, M. V. S. Kumar and P. K. Maiti, *J. Phys. Chem. B*, 2012, **116**, 4370–4376.
53 J. Aumanen, T. Kesti, V. Sundstrom, G. Teobaldi, F. Zerbetto, N. Werner, G. Richardt, J. van Heyst, F. Vogtle and J. Korppi-Tommola, *J. Phys. Chem. B*, 2010, **114**, 1548–1558.
54 X. Shi, I. Lee, X. Chen, M. Shen, S. Xiao, M. Zhu, J. R. Baker and S. H. Wang, *Soft Matter*, 2010, **6**, 2539–2545.
55 M. Lard, S. H. Kim, S. Lin, P. Bhattacharya, P. C. Ke and M. H. Lamm, *Phys. Chem. Chem. Phys.*, 2010, **12**, 9285–9291.
56 I. Tanis and K. Karatasos, *J. Phys. Chem. B*, 2009, **113**, 10984–10993.

57 I. Lee, I. J. Majoros, C. R. Williams, B. D. Athey and J. R. Baker Jr, *J. Comput. Theor. Nanosci.*, 2009, **6**, 54–60.
58 T. Chang, K. Pieterse, M. A. C. Broeren, H. Kooijman, A. L. Spek, P. A. J. Hilbers and E. W. Meijer, *Chem.–Eur. J.*, 2007, **13**, 7883–7889.
59 Y. Peng and G. A. Kaminski, *J. Phys. Chem. B*, 2005, **109**, 15145–15149.
60 G. Teobaldi and F. Zerbetto, *J. Lumin.*, 2005, **111**, 335–342.
61 G. Teobaldi and F. Zerbetto, *J. Am. Chem. Soc.*, 2003, **125**, 7388–7393.
62 A. Quintana, E. Raczka, L. Piehler, I. Lee, A. Myc, I. Majoros, A. Patri, T. Thomas, J. Mule and J. Baker, *Pharm. Res.*, 2002, **19**, 1310–1316.
63 S. Pricl and M. Fermeglia, *Carbohydr. Polym.*, 2001, **45**, 23–33.
64 I. Lee, B. D. Athey, A. W. Wetzel and J. R. Baker Jr, *Molecular dynamics studies on folic acid and fluorescein-derivatized PAMAM dendrimers*, Hilton Head Island, South Carolina, USA, 2001.
65 G. M. Torrie and J. P. Valleau, *J. Comput. Phys.*, 1977, **23**, 187–199.
66 V. Maingi, V. Jain, P. V. Bharatam and P. K. Maiti, *J. Comput. Chem.*, 2012, **33**, 1997–2011, http://www.physics.iisc.ernet.in/~maiti/dbt/home.html.
67 D. A. Case, T. A. Darden, T. E. Cheatham III, C. L. Simmerling, J. Wang, R. E. Duke, R. Luo, M. Crowley, R. C. Walker, W. Zhang, K. M. Merz, B. Wang, S. Hayik, A. Roitberg, G. Seabra, I. Kolossváry, K. F. Wong, F. Paesani, X. Wu, S. Brozell, T. Steinbrecher, H. Gohlke, L. Yang, C. Tan, J. Mongan, V. Hornack, G. Cui, D. H. Mathews, M. G. Seetin, C. Sagui, V. Babin and P. A. Kollman, University of California, *AMBER 10*, San Francisco, 2008.
68 G. J. M. Koper, M. H. P. Van Genderen, C. Elissen-Roman, M. W. P. L. Baars, E. W. Meijer and M. Borkovec, *J. Am. Chem. Soc.*, 1997, **119**, 6512–6521.
69 R. C. van Duijvenbode, M. Borkovec and G. J. M. Koper, *Polymer*, 1998, **39**, 2657–2664.
70 D. Cakara, J. Kleimann and M. Borkovec, *Macromolecules*, 2003, **36**, 4201–4207.
71 V. A. Kabanov, A. B. Zezin, V. B. Rogacheva, Z. G. Gulyaeva, M. F. Zansochova, J. G. H. Joosten and J. Brackman, *Macromolecules*, 1999, **32**, 1904–1909.
72 Y. Niu, L. Sun and R. M. Crooks, *Macromolecules*, 2003, **36**, 5725–5731.
73 J. Wang, R. M. Wolf, J. W. Caldwell, P. A. Kollman and D. A. Case, *J. Comput. Chem.*, 2004, **25**, 1157–1174.
74 W. L. Jorgensen, J. Chandrasekhar, J. D. Madura, R. W. Impey and M. L. Klein, *J. Chem. Phys.*, 1983, **79**, 926–935.
75 H. J. C. Berendsen, J. P. M. Postma, W. F. van Gunsteren, A. DiNola and J. R. Haak, *J. Chem. Phys.*, 1984, **81**, 3684–3690.
76 L. Verlet, *Phys. Rev.*, 1967, **159**, 98–103.
77 J. P. Ryckaert, G. Ciccotti and H. J. C. Berendsen, *J. Comput. Phys.*, 1977, **23**, 327–341.
78 T. Darden, D. York and L. Pedersen, *J. Chem. Phys.*, 1993, **98**, 10089–10092.
79 W. Humphrey, A. Dalke and K. Schulten, *J. Mol. Graphics*, 1996, **14**, 33–38.
80 S. Kumar, J. M. Rosenberg, D. Bouzida, R. H. Swendsen and P. A. Kollman, *J. Comput. Chem.*, 1992, **13**, 1011–1021.
81 A. Grossfield, http://membrane.urmc.rochester.edu/content/wham, version 2.0.6, 2004.
82 J. Srinivasan, T. E. Cheatham III, P. Cieplak, P. A. Kollman and D. A. Case, *J. Am. Chem. Soc.*, 1998, **120**, 9401–9409.
83 G. M. Pavan, M. A. Kostiainen and A. Danani, *J. Phys. Chem. B*, 2010, **114**, 5686–5693.
84 G. M. Pavan, P. Posocco, A. Tagliabue, M. Maly, A. Malek, A. Danani, E. Ragg, C. V. Catapano and S. Pricl, *Chem.–Eur. J.*, 2010, **16**, 7781–7795.
85 D. Ouyang, H. Zhang, D. P. Herten, H. S. Parekh and S. C. Smith, *J. Phys. Chem. B*, 2010, **114**, 9220–9230.
86 D. Ouyang, H. Zhang, H. S. Parekh and S. C. Smith, *Biophys. Chem.*, 2011, **158**, 126–133.
87 R. Esfand and D. A. Tomalia, *Drug Discovery Today*, 2001, **6**, 427–436.
88 T. J. Prosa, B. J. Bauer, E. J. Amis, D. A. Tomalia and R. Scherrenberg, *J. Polym. Sci., Part B: Polym. Phys.*, 1997, **35**, 2913–2924.
89 R. Scherrenberg, B. Coussens, P. van Vliet, G. Edouard, J. Brackman, E. de Brabander and K. Mortensen, *Macromolecules*, 1998, **31**, 456–461.
90 C. Wu, *Mol. Simul.*, 2010, **36**, 1164–1172.
91 P. K. Maiti, T. Çagin, S. T. Lin and W. A. Goddard, *Macromolecules*, 2005, **38**, 979–991.
92 J. Rudnick and G. Gaspari, *J. Phys. A: Math. Gen.*, 1986, **19**, L191.
93 P. K. Maiti and R. Messina, *Macromolecules*, 2008, **41**, 5002–5006.
94 L. J. Twyman, A. E. Beezer, R. Esfand, M. J. Hardy and J. C. Mitchell, *Tetrahedron Lett.*, 1999, **40**, 1743–1746.
95 A. E. Beezer, A. S. H. King, I. K. Martin, J. C. Mitchel, L. J. Twyman and C. F. Wain, *Tetrahedron*, 2003, **59**, 3873–3880.
96 A. S. Chauhan, S. Sridevi, K. B. Chalasani, A. K. Jain, S. K. Jain, N. K. Jain and P. V. Diwan, *J. Controlled Release*, 2003, **90**, 335–343.
97 R. K. Tekade, T. Dutta, V. Gajbhiye and N. K. Jain, *J. Microencapsulation*, 2009, **26**, 287–296.
98 B. Devarakonda, D. P. Otto, A. Judefeind, R. A. Hill and M. M. De Villiers, *Int. J. Pharm.*, 2007, **345**, 142–153.
99 G. Pistolis, A. Malliaris, D. Tsiourvas and C. M. Paleos, *Chem.–Eur. J.*, 1999, **5**, 1440–1444.
100 I. Bodnar, A. S. Silva, R. W. Deitcher, N. E. Weisman, Y. H. Kim and N. J. Wagner, *J. Polym. Sci., Part B: Polym. Phys.*, 2000, **38**, 857–873.

